Journal of Engineering Mathematics **32:** 1–18, 1997.

Microwave heating of ceramic laminates

J.A. PELESKO and G.A. KRIEGSMANN
Department of Mathematics, Center for Applied Mathematics and Statistics, New Jersey Institute of Technology, University Heights, Newark, NJ 07102, U.S.A.

Received 22 January 1996; accepted in revised form 5 September 1996

Abstract. The microwave heating of a ceramic laminate composed of three layers is modeled and analyzed. Two materials with widely disparate effective electrical conductivities comprise the laminate. The ratio of these conductivities is exploited as a small parameter in the development of an asymptotic theory. Two physically distinct situations are considered. In the first, a low-loss ceramic is surrounded by lossy material. Here, the asymptotic theory yields simplified equations which are reduced to a nonlinear Volterra integral equation. The integral equation is amenable to analysis, and the results are physically interpreted. In the second situation, a lossy material is surrounded by a low-loss material. In this case the asymptotic theory yields simplified equations which are analyzed through numerical techniques. Again, the results are physically interpreted to attain insight into the dynamics and parameter dependence of the microwave heating of ceramic laminates.

Key words: microwave heating, ceramics, laminates, electrical conductivity, asymptotics

1. Introduction

In recent years, microwave processing of ceramic materials has become an area of intense activity [1]. Investigators in the field hope to produce efficiently high-quality materials and products. However, they are faced with numerous difficulties. Some materials of commercial interest, such as alumina, are essentially transparent to microwaves, while others, such as silicon carbide, absorb microwaves readily. Many investigators have explored 'hybrid' heating techniques in an effort to overcome the difficulties associated with processing either type of material [2–3]. Most hybrid heating schemes involve the simultaneous heating of two electrically and thermally disparate materials. When these materials are in contact, the scheme can be viewed as the heating of a ceramic laminate. In this paper we explore two such situations.

We consider first the microwave heating of microwave transparent, or low-loss, materials. Here, two key difficulties arise. Since the material is essentially transparent to microwaves, a large amount of power is required to heat these materials to processing temperatures. Further, the electrical conductivity of low-loss ceramics typically varies exponentially with temperature. This often leads to thermal runaway. In thermal runaway, the temperature of the material increases uncontrollably once the temperature of the material exceeds some critical temperature. Unfortunately, the critical temperature is often below the desired processing temperature. One method for overcoming both of these difficulties is to surround the low-loss ceramic with a lossy susceptor. Since the susceptor absorbs microwave radiation readily, it heats the low-loss ceramic by conduction, and requires less power. Investigators have also observed that, when a susceptor is used, the critical temperature at which thermal runaway occurs is increased [3]. This may allow one to heat the low-loss ceramic to the desired processing temperature, while avoiding thermal runaway.

In the first part of this paper we model the heating of a low-loss ceramic through the use of a lossy susceptor. We exploit the ratio of the two materials' electrical conductivities as a small

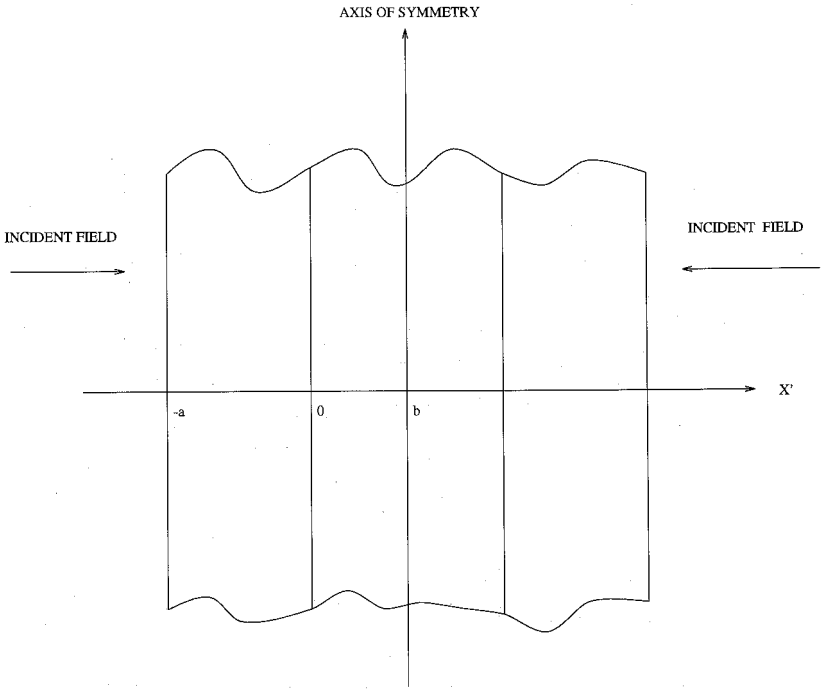

Figure 1. Sketch of the model configuration.

parameter in the development of an asymptotic theory. We illustrate how the use of a susceptor lowers the power requirements. Further, we show how the maximum stable temperature varies as a function of the thickness of the susceptor. We also note that thermal gradients within the low-loss ceramic are lower when a susceptor is employed than when the material is heated alone. This produces, in such processes as sintering, a more homogeneous material product [1].

In the second part of this paper we consider the microwave heating of lossy targets. Since microwaves heat volumetrically, a microwave-irradiated material is hotter inside than near the surface. A very important goal of microwave processing, as mentioned above for sintering, is the uniform heating of materials. Numerous investigators have placed low-loss insulation around lossy targets [2, 4] to reduce thermal gradients. This type of laminate is identical to the previous hybrid heating scheme with the roles of the low-loss and lossy materials reversed. Using the same asymptotic method as employed in the first part of this paper, we develop a theory for the microwave heating of an insulated lossy target. We show how the use of insulation dramatically reduces thermal gradients within the material. We also show that the use of insulation lowers the power requirements, and we determine how the maximum stable temperature varies as a function of the insulation thickness.

2. Formulation of the model

We begin by considering a ceramic laminate comprised of three thin isotropic ceramic slabs as shown in Figure 1. The outer two slabs are considered to be identical materials of equal thickness. Further, the composite is irradiated by identical microwaves from both sides. We

chose this symmetric radiation to simplify the analysis to follow; the system of governing equations is symmetric about the centerline of the laminate.

We further assume that the incident electromagnetic wave and the electric field within the materials are time-harmonic, while the temperature distribution in each material is time-dependent. While the governing equations do not admit such a solution, it has been shown in [5] that the equations we present are the leading-order equations of an asymptotic theory. This theory is based on the assumption that the time required for heat to diffuse an electromagnetic wavelength is much greater than the period of a microwave.

With these assumptions in mind, we first formulate the equations governing the temperature distributions in each material. The first material, a lossy ceramic, occupies the region $-a < x' < 0$, while the second, a low-loss ceramic, fills the region $0 < x' < b$. The axis of symmetry is taken to be at $x' = b$; hence we are modeling the microwave heating of a low-loss ceramic surrounded by lossy material. In this configuration the lossy materials are often referred to as 'susceptors', while the low-loss material is called the 'ceramic'. We adopt this convention. The temperatures of our susceptor, T_1, and ceramic, T_2, satisfy

$$\rho_1 c_1 \frac{\partial T_1}{\partial t'} = K_1 \frac{\partial^2 T_1}{\partial x'^2} + \frac{|E_1|^2}{2}\varsigma_1(T_1), \quad -a < x' < 0, \tag{1a}$$

$$\rho_2 c_2 \frac{\partial T_2}{\partial t'} = K_2 \frac{\partial^2 T_2}{\partial x'^2} + \frac{|E_2|^2}{2}\varsigma_2(T_2), \qquad 0 < x' < b. \tag{1b}$$

Here ρ denotes density, c specific heat, K thermal conductivity, $|E|^2$ the electric field intensity, and ς_j denotes the effective electrical conductivity of the jth material which is a known function of the temperature.

The susceptor and the ceramic are assumed to be in perfect thermal contact at $x' = 0$ and hence we impose the following boundary conditions at this interface

$$K_1 \frac{\partial T_1}{\partial x'} = K_2 \frac{\partial T_2}{\partial x'}, \quad x' = 0; \qquad T_1(0, t') = T_2(0, t'). \tag{2a, b}$$

At the left-hand boundary of the susceptor, $x' = -a$, we assume that heat is lost through both convection and radiation and hence impose

$$K_1 \frac{\partial T_1}{\partial x'} = h(T_1 - T_A) + s\epsilon(T_1^4 - T_A^4), \quad x' = -a, \tag{3a}$$

where h is a convective heat-transfer coefficient, s is the Stefan–Boltzmann constant, ϵ is the emissivity, and T_A is the ambient temperature of the surrounding environment. At the axis of symmetry, $x' = b$, we impose the condition

$$\frac{\partial T_2}{\partial x'} = 0, \quad x' = b. \tag{3b}$$

Finally, we assume that both slabs are initially at the ambient temperature of the environment, *i.e.*,

$$T_1(x', 0) = T_2(x', 0) = T_A. \tag{4}$$

Next, we formulate the equations governing the electric field. A plane, time-harmonic electromagnetic wave of frequency ω impinges upon the susceptor from the left. A portion of this wave scatters from the interface at $x' = -a$, a portion penetrates and heats the susceptor, a portion scatters from the interface at $x' = 0$, and a portion penetrates and heats the ceramic. At $x' = b$ we will impose 'no-flux' conditions on the electric field in keeping with the symmetry assumptions outlined above. In the free-space region $x' < -a$, the electric field is given by

$$\mathbf{E} = E_0[\exp(ik'x' - i\omega t') + \Gamma \exp(-ik'x' - i\omega t')]\mathbf{k}, \quad x' < -a, \tag{5}$$

where E_0 is the strength of the incident field, $k' = \omega/c$, c is the speed of light in free space, and Γ is the total reflection coefficient.

Within the laminate the electric field is given by $\mathbf{E} = [E_j(x')\exp(-i\omega t')]\mathbf{k}$, $j = 1, 2$, where $j = 1$ corresponds to the susceptor and $j = 2$, the ceramic. The function E_1 satisfies

$$\frac{\mathrm{d}^2 E_1}{\mathrm{d}x'^2} + k_1'^2\left[1 + \frac{i}{\omega\epsilon_1}\varsigma_1(T_1)\right]E_1 = 0, \quad -a < x' < 0 \tag{6a}$$

in the susceptor and E_2 satisfies

$$\frac{\mathrm{d}^2 E_2}{\mathrm{d}x'^2} + k_2'^2\left[1 + \frac{i}{\omega\epsilon_1}\varsigma_2(T_2)\right]E_2 = 0, \qquad 0 < x' < b \tag{6b}$$

in the ceramic. Here ϵ_j is the permitivity of the jth material, $k_j' = \omega/c\sqrt{\epsilon_j/\epsilon_0}$, and ϵ_0 is the permitivity of free space. The magnetic permeabilities of both materials are assumed identical to that of free space.

At the interface $x' = -a$ the tangential electric and magnetic fields are continuous, hence E_1 and its derivative are also continuous at $x' = -a$. Combining this fact with (5) and eliminating Γ, we find that E_1 satisfies

$$\frac{\mathrm{d}E_1(-a)}{\mathrm{d}x'} + ik'E_1(-a) = 2E_0ik'\exp(-ik'a). \tag{6c}$$

The same continuity assumption applied at $x' = 0$ yields the boundary conditions

$$E_1(0) = E_2(0); \qquad E_1'(0) = E_2'(0). \tag{6d, e}$$

Finally, the symmetry condition at $x' = b$ implies that

$$E_2'(b) = 0. \tag{6f}$$

Next, we choose dimensionless temperature and length scales, scale the electric field with the amplitude of the incident wave, and rewite the conductivities as their values at the ambient temperature, multiplied by a dimensionless function of the scaled temperatures. Further, we scale time with respect to the diffusive time of the ceramic. This yields the new variables

$$v = (T_1 - T_A)/T_A, \qquad u = (T_2 - T_A)/T_A, \qquad e_1 = E_1/E_0, \qquad e_2 = E_2/E_0,$$

$$\varsigma_1 = \sigma_1 g(v), \qquad \varsigma_2 = \sigma_2 f(u), \qquad t = \frac{K_2 t'}{\rho_2 c_2 b^2}, \qquad x = x'/b.$$

When we introduce these into (1–6), the following dimensionless parameters naturally arise

$$\mu = \frac{\rho_1 c_1}{\rho_2 c_2}, \qquad \gamma = \frac{K_2}{K_1}, \qquad p = \frac{b\sigma_2 E_0^2}{2hT_A}, \qquad \delta = \frac{\sigma_2}{\sigma_1}, \qquad B = \frac{hb}{K_2}, \qquad d = a/b,$$

$$R = (s\epsilon T_A^3)/h, \qquad k = k'b, \qquad k_1 = k_1'b, \qquad k_2 = k_2'b, \qquad \nu\sigma/(\omega\epsilon_1).$$

The parameters μ and γ are dimensionless ratios of material properties. The parameter p is a dimensionless ratio of power absorbed from the electric field and power lost at the boundaries by convection. The Biot number, B, measures the relative effects of convection and conduction, R measures the relative effects of convection and radiation, and δ is a dimensionless ratio of the two effective electrical conductivities of the ceramic at the ambient temperature. The parameters k, k_1, and k_2 are dimensionless wave numbers scaled with ceramic thickness, and finally ν is the ratio of the wavelength in the susceptor and the skin depth at the ambient temperature, T_A.

In terms of our dimensionless variables and parameters the governing equations for the temperatures become

$$\mu\gamma\frac{\partial v}{\partial t} = \frac{\partial^2 v}{\partial x^2} + \frac{pB\gamma}{\delta}g(v)|e_1|^2, \quad -d < x < 0, \tag{7a}$$

$$\frac{\partial u}{\partial t} = \frac{\partial^2 u}{\partial x^2} + pBf(u)|e_2|^2, \quad 0 < x < 1, \tag{7b}$$

$$\frac{\partial v}{\partial x} = \gamma\frac{\partial u}{\partial x}, \quad x = 0; \qquad v(0,t) = u(0,t), \tag{8a, b}$$

$$\frac{\partial v}{\partial x} = B\gamma L(v), \quad x = -d; \qquad L(v) = v + R\{(v+1)^4 - 1\}, \tag{9a, b}$$

$$\frac{\partial u}{\partial x} = 0, \quad x = 1; \qquad v(x,0) = u(x,0) = 0. \tag{9c, d}$$

Similarly, the equations governing the electric field become

$$\frac{\mathrm{d}^2 e_1}{\mathrm{d}x^2} + k_1^2[1 + i\nu g(v)]e_1 = 0, \quad -d < x < 0, \tag{10a}$$

$$\frac{\mathrm{d}^2 e_2}{\mathrm{d}x^2} + k_2^2[1 + i\nu\delta f(u)]e_2 = 0, \quad 0 < x < 1, \tag{10b}$$

$$\frac{\mathrm{d}e_1(-d)}{\mathrm{d}x} + ike_1(-d) = 2ik\exp(-ikd), \tag{10c}$$

$$e_1(0) = e_2(0); \qquad e_1'(0) = e_2'(0); \qquad e_2'(1) = 0. \tag{10d, e, f}$$

Equations (7–10) are the governing equations for our microwave-irradiated ceramic laminate. The appearance of the nonlinear dimensionless conductivity functions $g(v)$ and $f(u)$, and the nonlinear boundary condition (9c) precludes an exact solution to this system of equations.

In the next section we develop an asymptotic theory which gives an accurate approximation of the solutions to our model equations.

3. An asymptotic theory

We begin by recalling our assumptions regarding the electrical conductivities of the susceptor and the ceramic: the former is quite large, while the latter is very small. In applications such materials might be SiC and alumina, respectively. We find for this case that $\delta \sim 10^{-5}$. We also note that, for these materials, the ratio of their thermal conductivities, $\gamma \sim 10^{-2}$. We take δ to be a small parameter and order the remaining dimensionless parameters with respect to δ. In particular, we assume that μ, B, R, k, k_1, k_2 and ν are all $O(1)$ and order p and γ as

$$p = P\delta, \qquad \gamma = \alpha\delta^{1/2}. \tag{11}$$

Here P and α are assumed to be $O(1)$. This restriction on α is true for ceramics whose conductivity ratio is as discussed above.

Next we assume an expansion in powers of $\delta^{1/2}$ for u, v, e_1 and e_2, that is

$$v \sim v_0 + \delta^{1/2}v_1 + \delta v_2 + \cdots; \qquad u \sim u_0 + \delta^{1/2}u_1 + \delta u_2 + \cdots, \tag{12a, b}$$

$$e_1 \sim V_0 + \delta^{1/2}V_1 + \delta V_2 + \cdots; \qquad e_2 \sim U_0 + \delta^{1/2}U_1 + \delta U_2 + \cdots. \tag{12c, d}$$

Inserting (11–12) into (7–10), expanding the nonlinear terms in an asymptotic series, and equating to zero the coefficients of the powers of $\delta^{1/2}$, we obtain an infinite set of equations which sequentially determine the v_n, V_n, u_n and U_n. We list the first two equations for the v_n and u_n, and only the first equation for the V_n and U_n. These are the equations needed to determine the leading-order terms in the asymptotic approximation to the temperature and electric field in the laminate. They are

$$\frac{\partial^2 v_0}{\partial x^2} = 0, \quad -d < x < 0; \qquad \frac{\partial u_0}{\partial t} = \frac{\partial^2 u_0}{\partial x^2}, \quad 0 < x < 1, \tag{13a, b}$$

$$\frac{\partial v_0}{\partial x} = 0, \quad x = -d, 0; \qquad \frac{\partial u_0}{\partial x} = 0, \quad x = 1, \tag{13c, d}$$

$$v_0(0,t) = u_0(0,t); \qquad v_0(x,0) = u_0(x,0) = 0, \tag{13e, f}$$

$$\mu\alpha\frac{\partial v_0}{\partial t} = \frac{\partial^2 v_1}{\partial x^2} + BP\alpha g(v_0)|V_0|^2, \quad -d < x < 0, \tag{14a}$$

$$\frac{\partial u_1}{\partial t} = \frac{\partial^2 u_1}{\partial x^2}, \quad 0 < x < 1, \tag{14b}$$

$$\frac{\partial v_1}{\partial x} = \alpha BL(v_0), \quad x = -d; \qquad \frac{\partial u_1}{\partial x} = 0, \quad x + 1, \tag{14c, d}$$

$$v_1(0,t) = u_1(0,t); \qquad \frac{\partial v_1}{\partial x} = \alpha \frac{\partial u_0}{\partial x}, \quad x = 0; \qquad v_1(x,0) = u_1(x,0) = 0. \quad \text{(14e, f, g)}$$

and

$$\frac{\mathrm{d}^2 V_0}{\mathrm{d}x^2} + k_1^2[1 + i\nu g(v_0)]V_0 = 0, \quad -d < x < 0, \tag{15a}$$

$$\frac{\mathrm{d}^2 U_0}{\mathrm{d}x^2} + k_2^2 u_0 = 0, \quad 0 < x < 1, \tag{15b}$$

$$\frac{\mathrm{d}V_0(-d)}{\mathrm{d}x} + ikV_0(-d) = 2ik\exp(-ikd), \tag{15c}$$

$$V_0(0) = U_0(0); \qquad V_0'(0) = U_0'(0); \qquad V_0'(1) = 0. \tag{15d, e, f}$$

To begin our analysis we integrate Equation (13a) twice and apply the boundary condition (13c) to obtain $v_0 = v_0(t)$, *i.e.*, v_0 is a function of time only. Then, an examination of the electric-field equations (15a,b) reveals that U_0 and V_0 only depend parametrically upon t through $v_0(t)$. These equations are then linear and may be solved exactly. Due to the complexity of the analytical solutions we have placed them in Appendix A. Here we regard U_0 and V_0 as known functions of temperature and position and proceed to consider the leading-order equations for u_0 and v_0.

Next, we integrate Equation (14a) with respect to x over the interval $(-d, 0)$ and apply the boundary conditions (14c, f) to obtain

$$\mu d \frac{\mathrm{d}v_0}{\mathrm{d}t} = \frac{\partial u_0}{\partial x}(0,t) - BL(v_0) + BPg(v_0)\|V_0\|^2(v_0), \tag{16a}$$

$$\|V_0\|^2(v_0) = \int_{-d}^{0} |V_0|^2 \,\mathrm{d}x, \tag{16b}$$

where the dependence of V_0 on v_0 is indicated. Since $v_0 = v_0(t)$, it follows from (13e) that $u_0(0,t) = v_0(t)$. Inserting this into (16a), we obtain the nonlinear mixed boundary condition

$$\mu d \frac{\partial u_0}{\partial t} = \frac{\partial u_0}{\partial x} - BL(u_0) + BPg(u_0)\|V_0\|^2(u_0), \quad x = 0. \tag{17}$$

Finally, we observe that, Equations (13b), (13d), and (17), along with the initial condition (13f) constitute an initial-boundary-value problem for the leading-order temperature in the ceramic u_0. Once it is determined, the temperature in susceptor $v_0(t) = u_0(0,t)$ is known. Thus, the leading-order approximation of the temperature and electric field in the laminate is known.

4. Analysis of the reduced system

For the convenience of the reader we restate here the initial-boundary-value problem for $u_0(x,t)$. It is

$$\frac{\partial u_0}{\partial t} = \frac{\partial^2 u_0}{\partial x^2}, \quad 0 < x < 1, \tag{18a}$$

$$\mu d\frac{\partial u_0}{\partial t} = \frac{\partial u_0}{\partial x} - BL(u_0) + BPg(u_0)\|V_0\|^2(u_0), \quad x = 0, \tag{18b}$$

$$\frac{\partial u_0}{\partial x} = 0, \quad x = 1; \qquad u_0(x,0) = 0. \tag{18c, d}$$

The nonlinearities of the original problem now manifest themselves entirely in the boundary condition (18b). This boundary condition also has the additional feature of possessing a time derivative. We analyze this problem in two steps. In the first we consider the steady-state solutions of (18) and investigate their stability. Then we use these results to help analyze and interpret the dynamical solutions of (18).

4.1. STEADY-STATE SOLUTIONS

We begin by seeking steady-state solutions of (18). Setting the time derivatives equal to zero, integrating the resulting ordinary differential equation, and applying the boundary conditions, we find that steady-state solutions, denoted u_0^*, are independent of x and must satisfy

$$P = \frac{L(u_0^*)}{g(u_0^*)\|V_0\|^2(u_0^*)}. \tag{19}$$

In order to pursue the analysis further we must choose a specific form for the function g. Recall that g is the non-dimensional conductivity function for susceptor. Examination of conductivity data [6] for susceptors, such as SiC, reveals that g is an exponential function of temperature. Thus we take

$$g(u_0^*) = \mathrm{e}^{\beta_1 u_0^*}, \tag{20}$$

where the constant β_1 depends upon the particular material. Having chosen this exponential form for g, we may proceed with the analysis. In general we cannot explicitly solve (19) for u_0^* as a function of P. However, this can be done graphically as shown in Figure 2, where P is plotted as a function of u_0^*, and the axes are reversed. This power-response curve has the familiar S-shape first discussed in [7]. That is, depending on the value of the parameter P, there are one, two, or three steady-state solutions. In order to sketch Figure 2, we set the Biot number $B = 0{\cdot}01, k_1 = 0{\cdot}1, k_2 = 0{\cdot}15, \nu = 0{\cdot}1, d = 0{\cdot}1, \beta = 0{\cdot}8$, and $k = 0{\cdot}5$ unless otherwise noted.

We shall now analyze the linear stability of these steady-state solutions. Accordingly, we seek a solution to (18) of the form

$$u_0(x,t) = u_0^* + w(x)\,\mathrm{e}^{-\lambda^2 t}, \tag{21}$$

where $|w(x)| \ll 1$. Inserting this *ansatz* into (18), expanding the nonlinear terms in Taylor series, and omitting quadratic and higher-order terms in w we obtain the eigenvalue problem

$$\frac{\mathrm{d}^2 w}{\mathrm{d}x^2} + \lambda^2 w = 0, \tag{22a}$$

$$[\mu d\lambda^2 - Bg(u_0^*)\|V_0\|^2(u_0^*)P'(u_0^*)]w(0) + w'(0) = 0, \tag{22b}$$

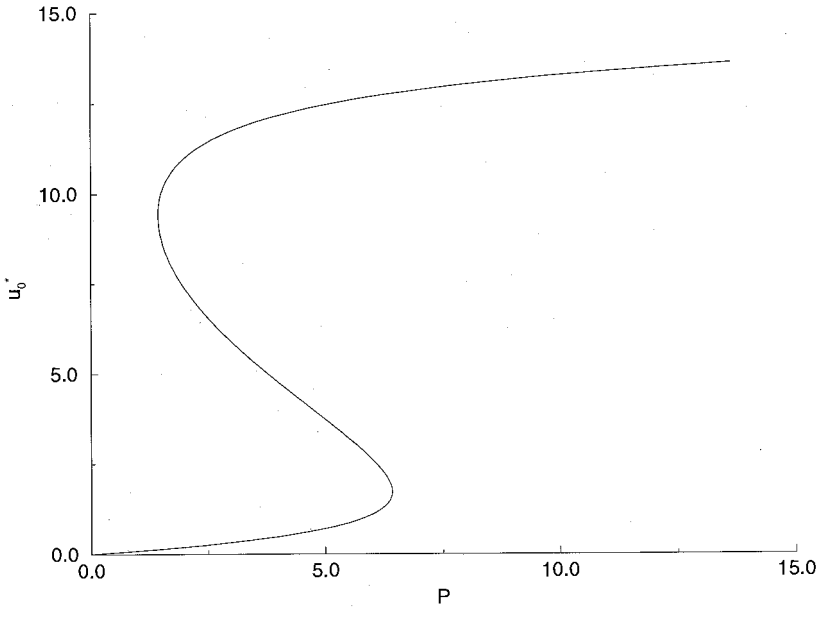

Figure 2. Sample power-response curve for susceptor ceramic.

$$w'(1) = 0, \tag{22c}$$

where we obtained $P'(u_0^*)$ by differentiating (19) with respect to u_0^*. This linear eigenvalue problem has a solution w when λ satisfies

$$\tan(\lambda) = -\mu d\lambda + \frac{Bg(u_0^*)\|V_0\|^2(u_0^*)P'(u_0^*)}{\lambda}. \tag{23}$$

The solutions of this equation in conjunction with (21) determine the stability of the perturbation w; if $\mathrm{Re}(\lambda^2) > 0 (< 0)$, then the steady-state u_0^* is linearly stable (unstable).

We shall first show that λ^2 is real. To demonstrate this, we multiply (22a) by the complex conjugate of w, integrate the resulting expression from 0 to 1, apply the boundary conditions (22b–d), and solve for λ^2. The result is

$$\lambda^2 = \frac{\|w'\|^2 + Bg(u_0^*)\|V_0\|^2(u_0^*)P'(u_0^*)}{\|w\|^2 + \mu d|w(0)|^2}, \tag{24}$$

where the norm $\|\ \|$ is as defined in (16b), with the limits of integration replaced by 0 and 1. Since the right-hand side of (24) is a real number, λ^2 is too, and we may conclude that λ is either purely real or purely imaginary. We further note that (22) with $\lambda = 0$ shows that zero is not an eigenvalue.

We shall now show that the steady-state solutions corresponding to the upper and lower branches of the s-shaped curve are stable, *i.e.*, $\lambda^2 > 0$. This follows from (24) and the fact that $P'(u_0^*) > 0$ on these branches, as can be seen from Figure 2.

For steady-state solutions lying on the middle branch we see from Figure 2 that $P'(u_0^*) < 0$. These solutions will be unstable if the numerator of (24) is negative. If this is the case, then $\lambda = ia$ and (23) becomes

$$\tanh(a) = -\mu da - \frac{Bg(u_0^*)\|V_0\|^2(u_0^*)P'(u_0^*)}{a}. \tag{25}$$

Equation (25) admits real roots; hence the middle branch is unstable. This is clear, for as a tends to zero (infinity), the right-hand side tends to positive (negative) infinity and intersects the graph of $\tanh(a)$.

4.2. Dynamics of the reduced system

In the previous subsection we analyzed the linear stability of our steady-state solutions. The linear-stability analysis yields a local result. In this subsection we explore the global behaviour of solutions by considering the dynamics of our reduced system. In particular, we rely on results due to Londen [8] and Roberts and Mann [9] to show that bounded solutions of (18) monotonically approach the stable steady-state solutions found in the previous subsection.

We begin by recasting the problem (18) as a nonlinear Volterra integral equation. This technique has been exploited by Mann and Wolf [10], Chambre [11] and others in the field of heat transfer, and in such diverse areas as superfluidity, population dynamics [12], and shape memory alloys [13]. To derive this integral equation, we apply the Laplace transform to the system (18), solve the resulting ordinary differential equation, use the convolution theorem to invert, and obtain

$$u_0(x,t) = \int_0^t F(u_0(0,\tau))H(x,t-\tau)\,\mathrm{d}\tau, \tag{26a}$$

where F is given by (22c),

$$H(x,t-\tau) = \frac{1}{1+\mu d} + \sum_{n=0}^{\infty} \frac{2\,\mathrm{e}^{-\alpha_n^2(t-\tau)}\,\cos(\alpha_n(1-x))}{\cos\,\alpha_n(1+\mu d+(\mu d\alpha_n))^2} \tag{26b}$$

and the $\alpha_n' s$ are the solutions of

$$\tan(\alpha) = -\mu d\alpha. \tag{26c}$$

Finally, we evaluate (26a) at $x = 0$ and obtain the Volterra equation

$$y(t) = \int_0^t F(y(\tau))\kappa(t-\tau)\,\mathrm{d}\tau, \tag{27}$$

where $\kappa(t-\tau) = H(0,t-\tau)$ and $y(t) = u_0(0,t)$, the temperature at the susceptor-ceramic boundary.

Noting that $\kappa(t)$ is bounded, nonincreasing, and fails to be $L_1(0,\infty)$, while F is continuous on the whole real line, we see that Londen's first theorem applies and we may conclude that any bounded solution of (27) satisfies

$$\lim_{t\to\infty} F(y(t)) = 0. \tag{28}$$

Therefore, bounded solutions of (28) approach one of the steady states found in the previous subsection.

Next, we wish to show monotonicity. First, differentiate (27) with respect to t and obtain

$$y'(t) = \kappa(0)F(y(t)) + \int_0^t F(y(\tau))\kappa'(t-\tau)\,\mathrm{d}\tau. \tag{29}$$

Denoting the first zero of F by y_e, we shall prove by contradiction that the solution is trapped between $y = 0$ and $y = y_e$. To see this, assume $y > y_e$ for some time t_1, then by continuity there exists a smallest time t_0 with $t_0 < t_1$ such that $y(t_0) = y_e$ and $y < y_e$ on $[0, t_0)$. But since evaluating (29) at $t = t_0$ yields $y'(t_0) < 0$, we see that this contradiction implies that $y < y_e$ for all t. Next, note that $y(0) = 0$ and $y'(0) > 0$ and assume $y < 0$ for some time t_1. Then there exists a smallest time $t_0 > 0$ such that $y(t_0) = 0$. Then, evaluating (27) at $t = t_0$, we find

$$0 = \int_0^{t_0} F(y(\tau))\kappa(t - \tau)\,\mathrm{d}\tau. \tag{30}$$

But we have just shown $y < y_e$, hence $F(y(t)) > 0$ on $[0, t_0]$, which implies that the integrand of (30) is positive, which is a contradiction.

Since we have shown that y is bounded between zero and the first zero of F, the first theorem of Roberts and Mann [9] applies and we conclude that bounded solutions of (27) increase monotonically. Combining the two results, we may conclude that bounded solutions of our reduced equations monotonically approach the steady-state solutions (18) u_0^* investigated in the previous subsection.

5. Analysis for a related geometry

Thus far, we have considered a low-loss ceramic surrounded by lossy susceptors. In applications the inverse situation often occurs. That is, in Figure 1 we take the two outer slabs to be low-loss ceramics and the middle slab to be lossy. In this situation the outer slabs may be referred to as 'insulators', while the inner slab is called the 'target'. Again, we adopt this convention. If we make the same symmetry assumptions as above, scale the governing equations in the same manner and perform the same asymptotic analysis, we again obtain a reduced system of equations which represent a leading-order asymptotic approximation to the temperatures of the slabs. We note that the scaling is done with respect to the material. In particular, the length scale is always chosen based on the length of the low-loss material. Our reduced system for this heating problem is

$$\frac{\partial u}{\partial t} = \frac{\partial^2 u}{\partial x^2}, \quad -1 < x < 0, \tag{31a}$$

$$\frac{\partial u}{\partial x} = BL(u), \quad x = -1, \tag{31b}$$

$$\mu d \frac{\partial u}{\partial t} + \frac{\partial u}{\partial x} = BPG(u), \quad x = 0, \tag{31c}$$

$$u(x, 0) = 0. \tag{31d}$$

Here u is the leading-order term of the asymptotic expansion for the solution in the insulator, V is the leading-order term for the electric field in the target and

$$G(u) = g(u) \int_0^d |V|^2\,\mathrm{d}x. \tag{31e}$$

An expression for V is derived in Appendix B.

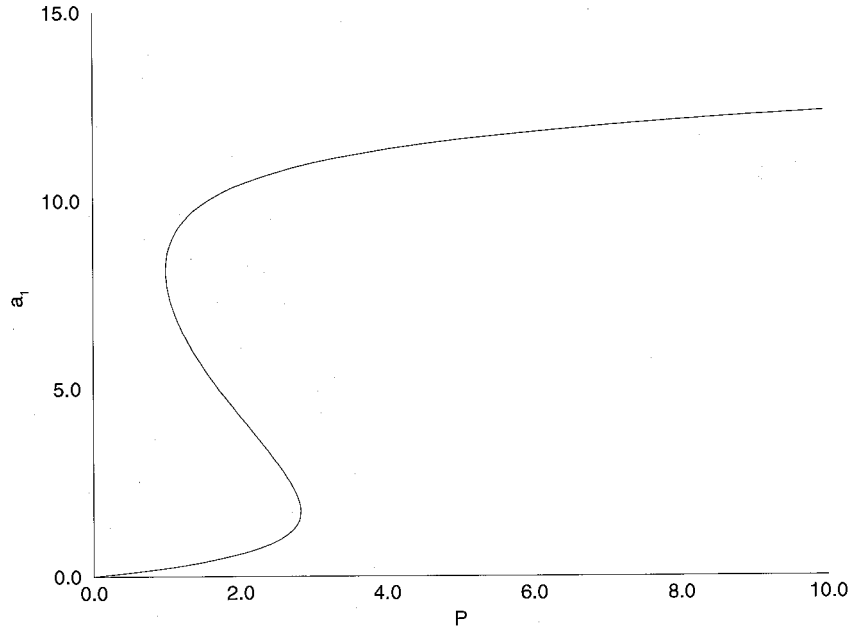

Figure 3. Sample power-response curve for insulated target.

We shall briefly analyze the steady-state solutions, their related stability and the dynamical solutions of this system in the following section.

5.1. STEADY-STATE SOLUTIONS

Again, we begin by seeking steady-state solutions to our initial-boundary-value problem (31). Setting the time derivatives equal to zero there, integrating the resulting ordinary differential equation, and applying the boundary conditions, we find that the steady-state temperature u^* is a linear function of position

$$u^*(x) = a_0 x + a_1, \tag{32a}$$

where the coefficients a_0 and a_1 satisfy:

$$a_0 = BL(a_1 - a_0); \qquad a_0 = PBG(a_1). \tag{32b, c}$$

Here we evaluated the norm of the electric field in G, using the temperature in the target, $u^*(0)$. We again assume that g is the exponential function (20) with an appropriate value of β_1.

We may eliminate a_0 from equations (32b, c) and obtain

$$P = L(a_1 - PBG(a_1))/G(a_1), \tag{33}$$

which is reminiscent of the power-response curve derived for the susceptor-ceramic. Since a_1 is the temperature in the target, Equation (33) represents a power-response curve for the target. In Figure 3 we plot the graph of (33) and again obtain an S-shaped curve. The linear profile may be recovered from Equation (32b).

The linear stability of these steady-state solutions will now be analyzed. Towards this end we let

$$u = u^*(x) + w(x)\,\mathrm{e}^{-\lambda^2 t}, \quad -1 < x < 0, \tag{34}$$

where again the perturbation $|w| \ll 1$. Inserting this *ansatz* into (31), expanding the nonlinear terms in Taylor series, and omitting quadratic and higher-order terms in w, we obtain the linear eigenvalue problem

$$\frac{\mathrm{d}^2 w}{\mathrm{d}x^2} + \lambda^2 w = 0, \quad -1 < x < 0, \tag{35a}$$

$$w'(-1) = BL'(u^*(-1))w(-1), \tag{35b}$$

$$-\mu d\lambda^2 w(0) + w'(0) = PBG'(u^*(0))w(0). \tag{35c}$$

Solving for w and applying the boundary conditions, we find that λ satisfies

$$\tan(\lambda) = -\lambda \frac{BPG'(a_1) - BL'(a_1 - a_0) + \mu d\lambda^2}{\mu d\lambda^2 BL'(a_1 - a_0) + B^2 PL'(a_1 - a_0)G'(a_1) + \lambda^2}. \tag{36}$$

The solutions of (36) in conjunction with (34) determine the stability of the perturbation w; if $\mathrm{Re}(\lambda^2) > 0 (< 0)$, then the steady-state u_0^* is stable (unstable).

We shall first demonstrate that λ^2 is real. To demonstrate this, we multiply (35a) by the complex conjugate of w, integrate the resulting expression from -1 to 0, apply the boundary conditions (35b–d), and solve for λ^2. The result is

$$\lambda^2 = \frac{\|w'\|^2 + |w(-1)|^2 BL'(a_1 - a_0) - ||w(0)|^2 PBG'(a_1)}{\mu d|w(0)|^2 + \|w'\|^2}. \tag{37}$$

Here the norm on w is over the interval $(-1, 0)$. Since the right-hand side of Equation (37) is real, we can again conclude that λ is either purely real or purely imaginary. A straightforward, but tedious analysis shows that real solutions to (37) exist for all points on our S-shaped curve. Hence stability is determined by imaginary solutions. If we set $\lambda = ia$ and insert this into (36), we obtain

$$\tanh(a) = -a \frac{BPG'(a_1) - BL'(a_1 - a_0) - \mu d a^2}{-\mu d a^2 BL'(a_1 - a_0) + B^2 PL'(a_1 - a_0)G'(a_1) - a^2}. \tag{38}$$

Again, the analysis of this equation is straightforward, but tedious. We do not repeat it here; rather we simply note that for points along the middle branch of our S-shaped curve, Equation (38) always has a real solution, hence the middle branch is unstable. Further, it may be shown that for points on the upper or lower branches of the S-shaped curve, Equation (38) never has a real solution; hence these branches are stable.

5.2. Dynamics for the insulated target

In the previous subsection we investigated the linear stability of steady-state solutions for the insulated-target configuration. We would like to extend this local analysis to determine the

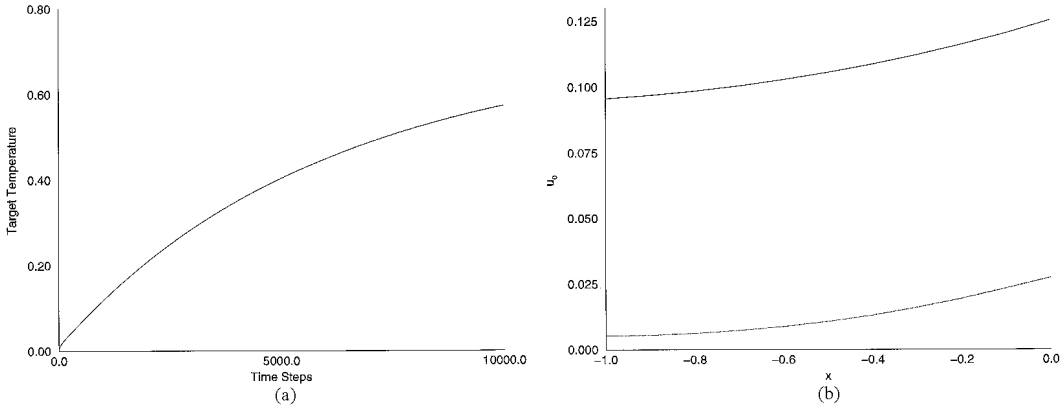

Figure 4. (a) Target temperature as a function of time, zero initial conditions; (b) temperature evolution in the insulation, zero initial conditions.

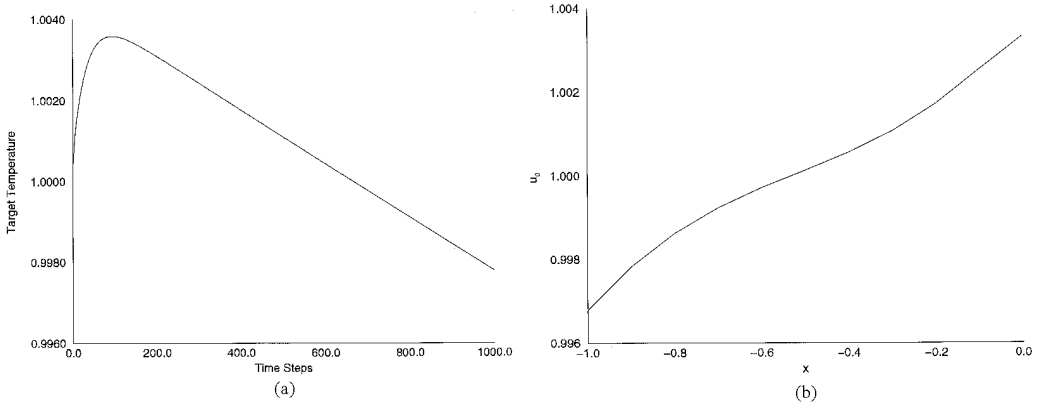

Figure 5. (a) Target temperature as a function of time, initial conditions above stable branch; (b) temperature evolution in the insulation, before loss effects have reached the target.

global behaviour of solutions, *i.e.* do solutions of our reduced system approach the steady-state solutions found in the previous subsection? If we again attempt to apply the Laplace transform to our reduced system and convert to an integral equation, we do not arrive at a single nonlinear integral equation, but a coupled pair of nonlinear Volterra inetgral equations. The analysis of such systems is daunting and here we resort to numerical techniques.

We apply an explicit finite-difference time-domain scheme to Equations (31). Some sample solutions are shown in Figures 4a and b. We note that, if the initial conditions are identically zero, the target temperature monotonically approaches either the upper or lower branch of the S-shaped curve according as the value of the power, P. If the initial conditions are not identically zero, the target temperature need not be a monotonic function of time. For example, if the initial conditions are constant, with a value slightly above a stable branch, the target temperature will initially increase before reversing direction and decreasing to the temperature of the nearest point on a stable branch. (See Figures 5a and b.) This is so because losses occur a finite distance away from the target; hence it takes finite time for the effect of those losses to be felt at the target. This is in contrast to the susceptor-ceramic configuration where the effect of losses was felt immediately and the temperature was always a monotonic function of time.

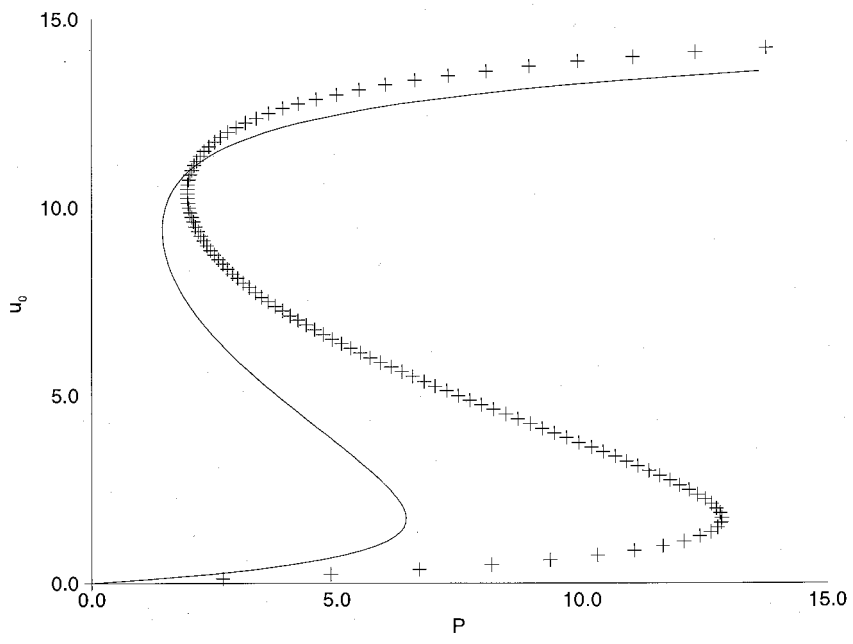

Figure 6. Power-response curves for susceptor ceramic, solid line is $d = 0{\cdot}1$, $+$ is $d = 0{\cdot}05$.

Finally, we note that, whether monotonically or not, the target temperature always approaches the nearest stable branch of the S-shaped curve.

6. Discussion

In order to interpret the results of our analysis, it will be useful to compare the heating of the composite structures considered above with the heating of solitary lossy and low-loss targets. The heating of solitary targets has been considered by several researchers; here we rely upon the results of Kriegsmann [5, 7], for purposes of comparison. Using an asymptotic analysis based on the assumption of a small Biot number, Kriegsmann derived a steady-state power-response curve for the heating of a solitary slab. Allowing θ to denote the temperature in the solitary slab, E the electric field, and assuming an expansion of the form

$$\theta \sim \theta_0 + B\theta_1 + \cdots \tag{39}$$

where B is the Biot number, Kriegsmann found that $\theta_0 = \theta_0(t)$ and in the steady-state satisfies

$$p = \frac{L(\theta_0)}{h(\theta_0)\|E_0\|^2}, \tag{40}$$

where here E_0 is the leading-order term in the expansion of the electric field and the norm is taken over the single slab. The function L and the parameter p are as in our model, and h is a non-dimensional conductivity function identical in meaning to our functions g and f.

First, we compare the results for the susceptor-ceramic model with the heating of a solitary low-loss ceramic. Recall that the response curve for the present susceptor-ceramic-susceptor

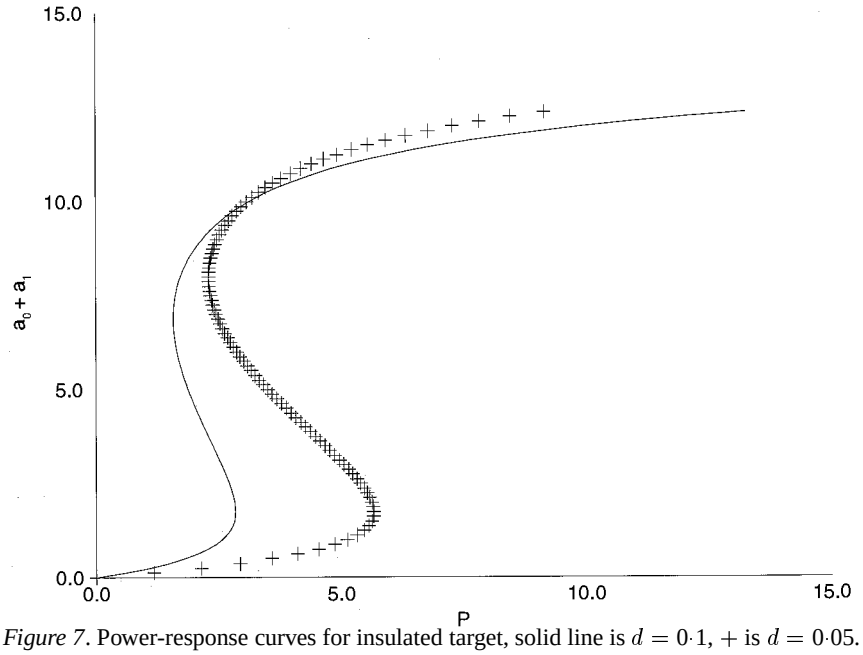

Figure 7. Power-response curves for insulated target, solid line is $d = 0{\cdot}1$, $+$ is $d = 0{\cdot}05$.

laminate is given by (19) under the assumption of an expansion of the form $u \sim u_0 + \delta^{1/2}u_1 + \cdots$. Since u_0 was found to depend only on time, any gradients within the low-loss ceramic must be $O(\delta^{1/2})$ in the steady-state. Form (39) we see that, for a solitary low-loss ceramic, thermal gradients are $O(B)$ in the steady state. For real materials $\delta^{1/2} \ll B$, which implies that the susceptor acts to smooth thermal gradients. Next, from (19) we note that for the laminate case the power axis is in terms of P, while from (40) we see that, for the solitary low-loss target, the power axis is scaled with p or, equivalently, $P\delta$. This implies that less power is necessary to reach a given temperature when a susceptor is used. This result is in agreement with qualitative experimental observations, [1–4]. Finally, in Figure 6, we plot our power-response curve for the laminate configuration for various values of the relative thickness, d. We make two observations. First, as the susceptor thickness is increased, the power requirements decrease. This is as expected from our comparison with the heating of a solitary low-loss target. Second, we note that the upper branch of the S-shaped curve is lower for larger d. This may have implications for thermal runaway. If initially the upper branch is above the desired processing temperature, the addition of a thicker susceptor may bring the branch down to desired processing temperatures. This may allow thermal runaway to be avoided; however the height of the upper branch also depends on material properties and these must be taken into account in any experimental situation. Again, these observations agree with qualitative experimental observations [1–4].

Finally, we compare the results for the insulated target with those of a solitary lossy target. The decreased power requirements and smoother thermal gradients follow from the same observations made in the susceptor-ceramic case. In Figure 7, we plot our power-response curve for the insulated target for various values of the relative thickness d. We again note that increased insulation lowers the power requirements. Further, we note that the upper branch of the S-shaped curve is again lower for larger d. If, for a given thickness of insulation, the upper

branch is at the processing temperature, this may imply that the addition of further insulation may actually increase the power requirements.

Appendix A

In this Appendix we present the exact solution to the reduced electric-field equations for the susceptor-ceramic-susceptor configuration. We find

$$V_0(x) = a(v_0)\exp(ik_1h(v_0)x) + b(v_0)\exp(-ik_1h(v_0)x), \tag{41a}$$

$$U_0(x) = c(v_0)\exp(ik_2x) + d(v_0)\exp(-ik_2x), \tag{41b}$$

where

$$h(v_0) = \sqrt{1 + i\nu g(v_0)}, \tag{42a}$$

$$a(v_0) = A(v_0)d(v_0); \qquad b(v_0) = B(v_0)d(v_0), \tag{42b, c}$$

$$c(v_0) = \exp(-2ik_2)d(v_0); \qquad d(v_0) = 2k\exp(-ikd)/C(v_0), \tag{42d, e}$$

$$A(v_0) = \frac{1}{2}\left(\left(\frac{k_2}{k_1h(v_0)} + 1\right)\exp(-2ik_2) + \left(1 - \frac{k_2}{k_1h(v_0)}\right)\right), \tag{43a}$$

$$B(v_0) = \frac{1}{2}\left(\left(1 - \frac{k_2}{k_1h(v_0)}\right)\exp(-2ik_2) + \left(1 + \frac{k_2}{k_1h(v_0)}\right)\right), \tag{43b}$$

$$\begin{aligned} C(v_0) \;=\; & A(v_0)(k + k_1h(v_0))\exp(-ik_1h(v_0)d) + \\ & + B(v_0)(k - k_1h(v_0))\exp(ik_1h(v_0)d). \end{aligned} \tag{43c}$$

Appendix B

In this Appendix we present the exact solution to the reduced electric-field equations for the insulated target configuration. We find

$$U_0(x) = a(v_0)\exp(ik_1x) + b(v_0)\exp(-ik_1x), \tag{44a}$$

$$V_0(x) = c(v_0)\exp(ik_2h(v_0)x) + d(v_0)\exp(-ik_2h(v_0)x), \tag{44b}$$

where

$$h(v_0) = \sqrt{1 + i\nu g(v_0)}, \tag{45a}$$

$$a(v_0) = A(v_0)d(v_0); \qquad b(v_0) = B(v_0)d(v_0), \tag{45b, c}$$

$$c(v_0) = \exp(-2ik_2h(v_0)d)d(v_0), \tag{45d}$$

$$d(v_0) = 2k\exp(-ik)/((k_1 + k)A(v_0)\exp(-ik_1) + (k - k_1)B(v_0)\exp(ik_1)) \tag{45e}$$

and

$$A(v_0) = (1/2)((k_2/k_1)h(v_0)(\exp(-2ik_2h(v_0)d) - 1) + \\ +(\exp(-2ik_2h(v_0)d) + 1)), \tag{46a}$$

$$B(v_0) = (-1/2)((k_2/k_1)h(v_0)(\exp(-2ik_2h(v_0)d) - 1) - \\ -(\exp(-2ik_2h(v_0)d) + 1)). \tag{46b}$$

Acknowledgement

The authors gratefully acknowledge financial support by the Air Force Office of Scientific Research under Grant # AFOSR F49620-94-1-0338 and the Department of Energy under Grant # DE-FG02-94ER25196.

References

1. W.H. Sutton, Key issues in microwave process technology. In: *Microwave Processing of Materials III*. Pittsburg, PA: MRS Symposium Proceedings (1992) pp. 3–20.
2. G.J. Vogt and W.P. Unruh, Microwave hybrid heating of alumina filaments. In: *Microwaves: Theory and Applications in Materials Processing II*. Westerville, Ohio: The American Ceramic Society (1993).
3. M.A. Janney, H.D. Kimrey and J.O. Kiggans, Microwave processing of ceramics: Guidelines used at the Oak Ridge National Laboratory. In: *Microwave Processing of Materials II*. Pittsburg, PA: Materials Research Society Symposium Proceedings (1992).
4. Y. Fang, D.K. Agrawal, D.M. Roy and R. Roy, Microwave sintering of calcium strontium zirconium phosphate ceramics. In: *Microwave Processing of Materials III*. Pittsburg, PA: Materials Research Society Symposium Proceedings (1992).
5. G.A. Kriegsmann, Microwave heating of dispersive media. *SIAM Journal of Applied Mathematics* 53 (1993) 655–669.
6. W.B. Westphal, Dielectric constant and loss measurements on high-temperature materials, Laboratory for Insulation Research Technical Report, MIT, October 1963.
7. G.A. Kriegsmann, Thermal runaway in microwave heated ceramics: A one-dimensional model. *Journal of Applied Physics* 71 (1992) 1960–1966.
8. S.O. Londen, On a nonlinear Volterra integral equation. *Journal of Differential Equations* 14 (1973) 106–120.
9. J.R. Roberts and W.R. Mann, On a certain nonlinear integral equation of the Volterra type. *Pacific J. Math.* 1 (1951) 431–445.
10. W.R. Mann and F. Wolf, Heat transfer between solids and gasses under nonlinear boundary conditions. *Quart. Appl. Math.* 11 (1951) 163–184.
11. P.L. Chambre, Nonlinear heat transfer problem. *Journal of Applied Physics* 30 (1959) 1683–1688.
12. P. Linz, *Analytical and Numerical Methods of Volterra Equations.* SIAM, Philadelphia (1985) 227 pp.
13. D.C. Lagoudas and Z. Ding, Modeling of thermoelectric heat transfer in shape memory alloy actuators: Transient and multiple cycle solutions, *International Journal of Engineering Sciences* (in press).